Enhanced Adaptive Polar-Linear Interpolation Aided Channel Estimation

Xianyu Chen and Ming Jiang, *Senior Member, IEEE*

***Abstract*— Among the numerous channel estimation (CE) techniques in the literature, pilot-aided channel estimation (PACE) has been widely employed, where interpolation methods can be used for reducing pilot overhead. The conventional family of linear interpolation (LI) based algorithms is easy to implement, but naturally results in residual interpolation errors even at high signal-to-noise ratios (SNR). In this letter, an enhanced adaptive polar linear interpolation (E-APLI) method is proposed, which exploits new algorithms of effective origin optimisation (EOO), adaptive angle gradient (AAG) and sparse channel detection (SCD). The proposed scheme is capable of outperforming a range of existing methods and adapting to any tap-delay-line (TDL) type channel model, in real-time, while maintaining a complexity as low as the traditional LI method.**

***Index Terms*— Channel estimation (CE), adaptive polar linear interpolation (APLI), expectation maximization (EM), sparse channel detection (SCD).**

I. Introduction

COHERENT detection has been widely used in existing wireless systems and is also likely in B4G/5G systems, for its significant performance gain over noncoherent detection. However, it requires accurate channel information which is usually acquired by the channel estimation (CE) module invoked at the receiver. In the literature, numerous CE methods have been proposed, including pilot-aided CE (PACE) [1], [2], decision-directed CE (DDCE) [3], [4], etc.

Among the existing CE techniques, PACE has shown attractive simplicity and effectiveness from implementational perspectives. In PACE-aided systems, interpolation techniques are typically needed, such as linear interpolation (LI), polynomial interpolation (PI), adaptive polar linear interpolation (APLI) [5], two-dimensional (2D) Wiener filtering [3], least mean square (LMS) filtering [2], Bayesian minimum mean square error channel estimation (BMMSE-CE) [6], and so on. Naturally, APLI offers notable improvements upon classical interpolation methods with the aid of the so-called sliding window (SW) mechanism. Though, it suffers from non-negligible residual interpolation errors even at high signal-to-noise ratios (SNR). On the other hand, methods like Wiener and LMS filtering often yield an increased complexity.

Against this background, we propose an enhanced APLI (E-APLI) scheme that exploits three new algorithms, referred to as effective origin optimisation (EOO), adaptive angle gradient (AAG) and sparse channel detection (SCD), respectively. *These new modules help to derive a more accurate effective origin (EO), improved adaptive interpolation steps and higher accuracy for conventional APLI, thus provide more robust interpolated channel coefficients regardless of the specific channel model and/or real-time channel conditions.* As a result, the proposed E-APLI-aided channel estimation (E-APLI-CE) scheme can outperform a range of existing techniques at a low computational complexity. Furthermore, it is readily applicable to any PACE schemes utilising frequency-domain (FD) interpolation, such as systems based on orthogonal frequency division multiplexing (OFDM).

The rest of this letter is organised as follows. In Section II, the proposed E-APLI-CE framework is introduced, followed by the relevant design details in Section III. The simulation results are provided in Section IV and our findings are concluded in Section V.

II. System Framework

The system framework of E-APLI-CE is illustrated in Fig. 1, where on the top of conventional APLI-CE [5], the new modules printed in gray colour are introduced. Assume that N data symbols are inserted between every two of the total P FD pilot symbols in a general OFDM system. At the k^{th} pilot subcarrier, the initial estimated FD channel transfer function (FD-CTF) $\hat{H}_{\rm LS}[k]$ is obtained for pilot $s_p[k]$ based on the least squares (LS) principle as

$$\hat{H}_{\rm LS}[k] = \frac{x[k]}{s_p[k]} = H[k] + \frac{s_p^*[k]}{|s_p[k]|^2}\cdot v[k],\ 0 \le k \le P-1, \quad (1)$$

where $(\cdot)^*$ denotes the conjugate operation, $x[k]$ is the symbol received after multi-path channel propagation, and $v[k]$ is the complex additive white Gaussian noise (AWGN) sample with zero mean and unit variance. Then, our new EOO procedure is invoked to calculate a reference point, c_k, which is referred to as the EO, as to be detailed in Section III-A.

In conventional APLI-CE [5], the origin shifting (OS) procedure is used to shift the origin of the complex plane to the EO. Then, the quadrant detector (QD) decides in which quadrant of the complex plane the origin-shifted effective LS estimates $\hat{H}'_{\rm LS}[\cdot]$ are located. Moreover, the quadrant-based phase adaptation (QPA) operation revises the phases of the origin-shifted LS estimates, resulting in the QPA-calibrated LS estimates denoted by $\hat{H}''_{\rm LS}[\cdot]$, as seen in the middle part of Fig. 1. Then, N polar-linearly interpolated FD-CTFs are

This work was supported in part by the General Project of National Natural Science Foundation of China under Grant 61771499 and in part by the Basic Research Project of Guangdong Provincial NSF under Grant 2016A030308008. (*Corresponding author: Ming Jiang*)

X. Chen and M. Jiang are with Sun Yat-sen University, Guangzhou 510275, China (e-mail: 734992689@qq.com; jiangm7@mail.sysu.edu.cn).

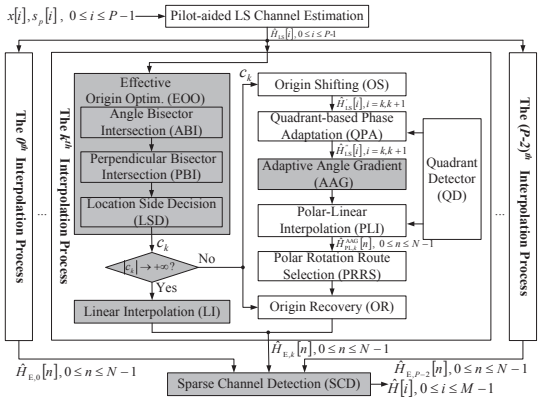

Fig. 1. The system framework of E-APLI-CE.

generated for the data symbols between the k^{th} and the $(k+1)^{th}$ pilots, as

$$\hat{H}_{\mathrm{PL},k}[n] = \hat{A}_{\mathrm{PL},k}[n] \cdot e^{j\hat{\alpha}_{\mathrm{PL},k}[n]},\ n = 0, \ldots, N-1, \quad (2)$$

where $\begin{cases} \hat{A}_{\mathrm{PL},k}[n] = \hat{A}''_{\mathrm{LS}}[k] + \Delta_A[k] \cdot (n+1) \\ \hat{\alpha}_{\mathrm{PL},k}[n] = \hat{\alpha}''_{\mathrm{LS}}[k] + \Delta_\alpha[k] \cdot (n+1) \end{cases}$ and the interpolation steps $\Delta_A[k]$ and $\Delta_\alpha[k]$ are defined by

$$\begin{cases} \Delta_A[k] = \frac{1}{N+1}(\hat{A}''_{\mathrm{LS}}[k+1] - \hat{A}''_{\mathrm{LS}}[k]) \\ \Delta_\alpha[k] = \frac{1}{N+1}(\hat{\alpha}''_{\mathrm{LS}}[k+1] - \hat{\alpha}''_{\mathrm{LS}}[k]) \end{cases}, \quad (3)$$

while $\hat{A}''_{\mathrm{LS}}[\cdot]$ and $\hat{\alpha}''_{\mathrm{LS}}[\cdot]$ denote the amplitude and the phase of $\hat{H}''_{\mathrm{LS}}[\cdot]$, respectively. However, the polar-linear interpolation (PLI) employed in APLI-CE invokes equal-interval interpolation steps specified by (3), thus cannot optimally adapt to the instantaneous and evolving FD-CTF contour on the complex plane. Hence, in the proposed E-APLI-CE of Fig. 1, a new module called AAG is added to improve the robustness of the PLI estimates through a *varying* interpolation step, as to be discussed in Section III-B.

Then, exploiting the AAG-enhanced PLI-based estimates $\hat{H}_{\mathrm{PL},k}[n]$, the polar rotation route selection (PRRS) [5] function selects the best polar rotation route (PRR), which is defined as the optimised 2D directional trajectory formed by the set of the aforementioned PLI-generated FD-CTF estimates $\hat{H}''_{\mathrm{LS}}[\cdot]$. With the aid of EO, they will be shifted back to their original locations with respect to the initial origin of the complex plane. Next, the new SCD module described in Section III-C is employed to reduce the interpolation-induced noise. Finally, we obtain the channel estimates $\hat{H}[i],\ 0 \le i \le M-1$, where $M = N \cdot P - N + P$, for data symbol detection.

III. Key Algorithm Design for E-APLI-CE

In this section, the three new algorithms designed for the proposed E-APLI-CE scheme are detailed.

A. The EOO Algorithm

The EOO algorithm steers the local position of the EO to ensure that each and every local portion of the estimated FD-CTF contour smartly fits its true versions. It includes three sub-modules, namely the angle bisector intersection (ABI), the perpendicular bisector intersection (PBI) and the location side decision (LSD) functions.

1) The ABI Sub-module: In order to determine the EO for the pilot estimate pair $\hat{H}_{\mathrm{LS}}[k]$ and $\hat{H}_{\mathrm{LS}}[k+1]$, which are given by (1), four consecutive pilot estimates $\hat{H}_{\mathrm{LS}}[l]$, where $l = \{k-1, k, k+1, k+2\}$, are exploited in the ABI procedure, as illustrated in Fig. 2(a).

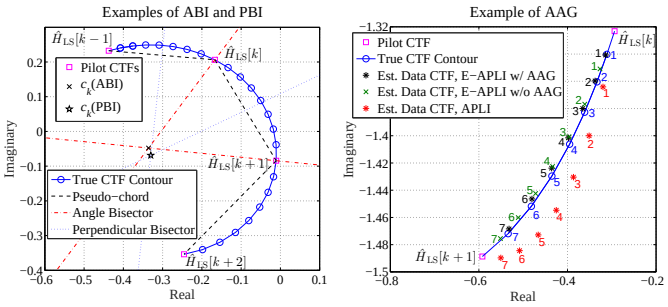

(a) EOO example. (b) AAG example.

Fig. 2. Examples of EOO and AAG.

More specifically, the angle bisector through $\hat{H}_{\mathrm{LS}}[k]$ is

$$y = \hat{H}_{\mathrm{LS}}[k] + k_1 n_1, \quad (4)$$

where $n_1 = \xi_1\left(\frac{r_{k,k-1}}{|r_{k,k-1}|} + \frac{r_{k,k+1}}{|r_{k,k+1}|}\right)$ with $\xi_1 \in \{1, -1\}$ suggests the possible directions of the specific angle bisector, $r_{i,j} = \hat{H}_{\mathrm{LS}}[j] - \hat{H}_{\mathrm{LS}}[i]$ indicates the pseudo-chord vector from point $\hat{H}_{\mathrm{LS}}[i]$ to point $\hat{H}_{\mathrm{LS}}[j]$, and $k_1 \in \mathbb{R}$. Similarly, the angle bisector through $\hat{H}_{\mathrm{LS}}[k+1]$ is

$$y = \hat{H}_{\mathrm{LS}}[k+1] - k_2 n_2, \quad (5)$$

where $n_2 = \xi_1\left(\frac{r_{k+1,k}}{|r_{k+1,k}|} + \frac{r_{k+1,k+2}}{|r_{k+1,k+2}|}\right)$ and $k_2 \in \mathbb{R}$. Then, the optimised version of the EO c_k, which is in fact the intersection point of the two angle bisectors denoted by (4) and (5), can be calculated by $c_k = \hat{H}_{\mathrm{LS}}[k] + k_1 n_1 = \hat{H}_{\mathrm{LS}}[k+1] - k_2 n_2$. After some derivations, we have

$$c_k = \frac{r_{k,k+1} n_2^* - r_{k,k+1}^* n_2}{n_1 n_2^* - n_1^* n_2} n_1 + \hat{H}_{\mathrm{LS}}[k]. \quad (6)$$

Then, the ABI-related c_k in (6) can be used as the EO for $\hat{H}_{\mathrm{LS}}[k]$ and $\hat{H}_{\mathrm{LS}}[k+1]$, as exemplified in Fig. 2(a).

2) The PBI Sub-module: The PBI procedure determines an improved EO based on the perpendicular bisector theory. Given three LS-based CTF estimates, $\hat{H}_{\mathrm{LS}}[l],\ l = \{k-1, k, k+1\}$, the perpendicular bisector of the pseudo-chord connecting $\hat{H}_{\mathrm{LS}}[k-1]$ and $\hat{H}_{\mathrm{LS}}[k]$ is defined by

$$z = x + k_1 n_1, \quad (7)$$

where $x = \frac{\hat{H}_{\mathrm{LS}}[k-1] + \hat{H}_{\mathrm{LS}}[k]}{2}$, $n_1 = \xi_2\left(\frac{r_{k,k-1}}{|r_{k,k-1}|}\right)$ indicates the direction of perpendicular bisector with $\xi_2 \in \{\sqrt{-1}, -\sqrt{-1}\}$, and $k_1 \in \mathbb{R}$. Similarly, the perpendicular bisector of the pseudo-chord connecting $\hat{H}_{\mathrm{LS}}[k]$ and $\hat{H}_{\mathrm{LS}}[k+1]$ is

$$z = y - k_2 n_2, \quad (8)$$

where $y = \frac{\hat{H}_{\mathrm{LS}}[k] + \hat{H}_{\mathrm{LS}}[k+1]}{2}$, $n_2 = \xi_2\left(\frac{r_{k+1,k}}{|r_{k+1,k}|}\right)$ and $k_2 \in \mathbb{R}$. Then, the intersection point of the two perpendicular bisectors denoted by (7) and (8) can be calculated by $c_k = x + k_1 n_1 = y - k_2 n_2$, yielding

$$c_k = \frac{(y-x) n_2^* - (y^* - x^*) n_2}{n_1 n_2^* - n_1^* n_2} n_1 + x, \quad (9)$$

which can then be used as an improved EO, as illustrated in Fig. 2(a).

3) The LSD Sub-module: Since FD-CTFs are the discrete Fourier transform (DFT) of channel impulse responses (CIR), meaning that they are the combination of CIR coefficients with clockwise-rotated phases, the FD-CTF contour is likely clockwise. This implies that c_k, as the EO, is usually at the right-hand side of the pseudo-chord vector $r_{k,k+1}$. However, in the unlikely event that the EO generated by ABI or PBI happens to be at the left-hand side of $r_{k,k+1}$, it would mislead the remaining CE procedure. Hence, it is necessary to judge at which side the EO is located with respect to $r_{k,k+1}$, which constitutes the task of the LSD sub-module. Specifically, we define an LSD control factor

$$\beta = \frac{-j \cdot r_{k,k+1}}{c_k - \hat{H}_{\mathrm{LS}}[k+1]}, \tag{10}$$

where $-j \cdot r_{k,k+1}$ is a vector perpendicular to $r_{k,k+1}$ with its direction pointing towards the right-hand side of $r_{k,k+1}$. Furthermore, denote $\angle\beta$ as the angle between $-j \cdot r_{k,k+1}$ and $c_k - \hat{H}_{\mathrm{LS}}[k+1]$. If $\Re(\beta) > 0$, we can infer that the EO is at the right-hand side of $r_{k,k+1}$, which justifies its use for next operations. Otherwise, this specific EO should be abandoned and the conventional APLI module is activated as a fall-back solution for deriving a new EO. If APLI fails to find a satisfying EO in its constrained search, we set $|c_k| = +\infty$ and employ the LI operator of Fig. 1 as the baseline approach.

Finally, we summarise the proposed EOO method in Algorithm 1, where an empirical parameter ρ is introduced to determine the activation of ABI, PBI or APLI procedures.

Algorithm 1 Effective Origin Optimisation (EOO) Algorithm

1: **Initialisation:** Obtain $\hat{H}_{\mathrm{LS}}[l],\ l = k-1, k, k+1, k+2$. Set $\omega_1 = \angle(\frac{r_{k,k+1}}{r_{k-1,k}})$, $\omega_2 = \angle(\frac{r_{k+1,k+2}}{r_{k,k+1}})$. Select the values of ρ, the minimum SW size $W_{\min}$ and the maximum SW size $W_{\max}$.
2: Calculate (6) with $\hat{H}_{\mathrm{LS}}[l],\ l = k-1, k, k+1, k+2 \ \Rightarrow\ c_k^{\mathrm{ABI}}$.
3: **if** $0 < \{|\omega_1|, |\omega_2|\} < \rho$ **and** $\Re(\beta) > 0$ in (10), **then goto** Step 17.
4: **if** $0 < |\omega_1| < \rho$ **and** $|\omega_2| \geq \rho$, **then**
5: Calculate (9) with $\hat{H}_{\mathrm{LS}}[l],\ l = k-1, k, k+1 \ \Rightarrow\ c_k^{\mathrm{PBI}}$.
6: **else if** $0 < |\omega_2| < \rho$ **and** $|\omega_1| \geq \rho$, **then**
7: Calculate (9) with $\hat{H}_{\mathrm{LS}}[l],\ l = k, k+1, k+2 \ \Rightarrow\ c_k^{\mathrm{PBI}}$.
8: **end if**
9: **if** c_k^{PBI} exists **and** $\Re(\beta) > 0$ in (10), **then goto** Step 17.
10: **else**
11: **for** $W = W_{\min} : 2 : W_{\max}$
12: Calculate (7) in [5] $\Rightarrow\ c_k^{\mathrm{APLI}}$.
13: **if** $\Re(\beta) > 0$ in (10), **then goto** Step 17.
14: **end for**
15: Set $|c_k| = +\infty$.
16: **end if**
17: **Return:** c_k as the derived EO.

B. AAG-aided PLI

Wireless channels are typically time-dispersive and frequency-selective, resulting in instantaneous fluctuations in FD-CTFs. In comparison to conventional APLI, where a fixed PLI step is used, the proposed AAG module shown in Fig. 1 invokes a fine adaptation to the gradient of the local FD-CTFs' instantaneous variation. This is achieved by adapting the PLI step for a better fit to the local CTFs' evolving trend. We define a gradient coefficient λ_k for the k^{th} pilot as

$$\lambda_k^{2(N+1)} = \frac{|\hat{H}''_{\mathrm{LS}}[k+2] - \hat{H}''_{\mathrm{LS}}[k+1]|}{|\hat{H}''_{\mathrm{LS}}[k] - \hat{H}''_{\mathrm{LS}}[k-1]|} \tag{11}$$

and a unit phase φ_k as

$$\varphi_k = \frac{\hat{\alpha}''_{\mathrm{LS}}[k+1] - \hat{\alpha}''_{\mathrm{LS}}[k]}{\sum_{i=0}^{N} \lambda_k^i}. \tag{12}$$

Compared with the PLI method that uses an equal-distance interpolation step $\Delta_\alpha[k]$ defined in (3), AAG utilises a gradient-based varying interpolation step, thus yielding an improved PLI estimate as

$$\hat{\alpha}_{\mathrm{PL},k}^{\mathrm{AAG}}[n] = \hat{\alpha}''_{\mathrm{LS}}[k] + \varphi_k \sum_{i=0}^{n} \lambda_k^i = \hat{\alpha}_{\mathrm{PL},k}^{\mathrm{AAG}}[n-1] + \Delta_\alpha^{\mathrm{AAG}}[n], \tag{13}$$

where $\Delta_\alpha^{\mathrm{AAG}}[n] = \varphi_k \lambda_k^n$ denotes the n^{th} AAG interpolation step. Then, by replacing $\hat{\alpha}_{\mathrm{PL},k}[n]$ in (2) with $\hat{\alpha}_{\mathrm{PL},k}^{\mathrm{AAG}}[n]$ in (13), we can obtain the AAG-enhanced PLI estimates $\hat{H}_{\mathrm{PL},k}^{\mathrm{AAG}}[n]$ well matching the true FD-CTFs, as exemplified in Fig. 2(b).

C. Sparse Channel Detection

As a further enhancement, a new method called SCD is designed to exploit the characteristics of the sparsity of wireless CIR. It can robustly perceive the zero-valued CIR taps without *a priori* channel information like the channel's maximum delay spread. Specifically, we exploit the principle of expectation maximization (EM) [7] to force specific CIR taps to zeros for noise reduction in E-APLI-CE.

As the input to SCD, the vector $\hat{\mathbf{H}}_{\mathrm{E}}$ seen at the lower part of Fig. 1 is first converted to $\hat{\mathbf{h}}_{\mathrm{E}}$ by inverse discrete Fourier transform (IDFT). Since the FD interpolation noise typically varies slowly from one subcarrier to the next, the corresponding time domain (TD) noise will mainly concentrate on low-index CIRs, implying that the noise variances at lower part of the CIR vector will be higher than those at higher part. Thus, the elements of $\hat{\mathbf{h}}_{\mathrm{E}}$ may be categorised into three groups for different treatments. The first group contains high-variance AWGN, which is complex Gaussian distribution (CGD) with zero mean and variance $\frac{\sigma_1^2}{2}$, $\mathcal{CN} \sim (0, \frac{\sigma_1^2}{2})$. The second group is low-variance AWGN, $\mathcal{CN} \sim (0, \frac{\sigma_2^2}{2})$. The third group corresponds to the sum of AWGN and non-zero CIR coefficients, $\mathcal{CN} \sim (0, \frac{\sigma_3^2}{2})$. We use $\phi(x|\frac{\sigma_k^2}{2}) = \frac{1}{\pi\sigma_k^2} \exp^{\frac{-|x|^2}{\sigma_k^2}}$ $(k = 1, 2, 3)$ to denote CGD's probability distribution function (PDF), where σ_k^2 are parameters to be iteratively estimated and improved during the SCD procedure, which is summarised in Algorithm 2.

IV. Simulation Results and Complexity Analysis

As an example, the 9-path LTE EVA channel model [8] was used. An Alamouti space-time block coded (STBC) 2×2 OFDM system was considered, assuming $N_{\mathrm{D}} = 2048$ and 64 quadrature amplitude modulation (64-QAM). To focus on the evaluation on CE, channel coding was not invoked. Similar to LTE PDSCH transmissions [9], we used FD and TD pilot

Algorithm 2 Sparse Channel Detection (SCD) Algorithm

1: **Initialisation:** Set $\hat{\sigma}_1^2 = 10^{\mathbb{U}(-3,-2)}$, $\hat{\sigma}_2^2 = 10^{\mathbb{U}(-5,-4)}$, and $\hat{\sigma}_3^2 = 10^{\mathbb{U}(-1,0)}$, where $\mathbb{U}(a,b)$ denotes a random number generator of uniform distribution between a and b. Randomly select β_k $(k = 1,2,3)$ that satisfy $\sum_{k=1}^{3}\beta_k = 1$ and $\beta_k \geq 0.1$, where β_k represents the *a priori* probability of an element in $\hat{\mathbf{h}}_{\mathrm{E}}$ belonging to the k-th CIR group. Set the to-be-estimated CIR vector $\hat{h}[j] = 0$ $(j = 0,\ldots,N_{\mathrm{D}}-1)$, where N_{D} is the DFT size.

2: Obtain $\hat{h}_{\mathrm{E}}[j] = \mathrm{IDFT}\big(\hat{\mathbf{H}}_{\mathrm{E}}\big),\ j = 0,\ldots,N_{\mathrm{D}}-1.$

3: **E Step:** Calculate contributions of the three CIR groups at each subcarrier

$$\hat{\gamma}_{jk} = \frac{\beta_k \phi(\hat{h}_{\mathrm{E}}[j]|\frac{\hat{\sigma}_k^2}{2})}{\sum_{k=1}^{3}\left[\beta_k \phi(\hat{h}_{\mathrm{E}}[j]|\frac{\hat{\sigma}_k^2}{2})\right]},\ j = 0,\ldots,N_{\mathrm{D}}-1;\ k = 1,2,3. \quad (14)$$

4: **M Step:** Based on (14), update the estimated parameters by

$$\hat{\sigma_k^2} = \frac{\sum_{j=0}^{N_{\mathrm{D}}-1}\hat{\gamma}_{jk}|\hat{h}_{\mathrm{E}}[j]|^2}{\sum_{j=0}^{N_{\mathrm{D}}-1}\hat{\gamma}_{jk}},\ \beta_k = \frac{\sum_{j=0}^{N_{\mathrm{D}}-1}\hat{\gamma}_{jk}}{N_{\mathrm{D}}},\ k = 1,2,3. \quad (15)$$

5: Repeat Steps 3 and 4 until the algorithm converges, meaning that the value changes of $\beta_k,\ k = 1,2,3$ are all less than a small number, such as $\epsilon = 10^{-6}$.

6: **for** $j = 0 : N_{\mathrm{D}}-1$ **do**

7: **if** $\hat{\gamma}_{j3} > \hat{\gamma}_{j1}$ **and** $\hat{\gamma}_{j3} > \hat{\gamma}_{j2}$, **then** $\hat{h}[j] = \hat{h}_{\mathrm{E}}[j]$.

8: **end for**

9: **Return:** FD-CTF estimates $\hat{H}[j] = \mathrm{DFT}\big(\hat{h}[j]\big),\ j = 0,\ldots,N_{\mathrm{D}}-1.$

spacings of 6 subcarriers and 7 OFDM symbols, respectively, indicating a very low pilot overhead of about 2.38%. For fair comparison, all benchmark schemes apply the same pilot pattern. Furthermore, we set $W_{\min} = 4$, $W_{\max} = 20$ and $\rho = \frac{\pi}{2}$ in Algorithm 1.

In Fig. 3, the mean square error (MSE) and block error rate (BLER) performances recorded for different CE schemes are compared assuming a user equipment (UE) velocity of 30km/h. One block is constituted by 256 subcarriers and 14 OFDM symbol durations, corresponding to about 20 allocated resource blocks (RB) in LTE systems. Note that the performance of E-APLI-CE is not sensitive to the initial values of $\{\sigma_k^2, \beta_k\}$ $(k = 1,2,3)$ used in Algorithm 2. In Table I, where for each E_b/N_0 value we tested 100 combinations of randomly selected $\{\sigma_k^2, \beta_k\}$, we can see that the standard deviations of the MSE results are only up to the order of 10^{-6} for a wide range of E_b/N_0. On the other hand, as shown in Fig. 3(a) and Fig. 3(b), E-APLI significantly outperforms LI, PI and conventional APLI [5]. Furthermore, in the cascaded one-dimensional MMSE (C1D-MMSE) CE [3] scheme, each FD-CTF is estimated first with $N_{\mathrm{MMSE}}^{\mathrm{FD}} = 4$ nearest FD pilots and then with $N_{\mathrm{MMSE}}^{\mathrm{TD}} = 2$ nearest TD pilots, and it assumes that the power delay profile (PDP) and Doppler spread of the channel are *a priori* known, which, however, are not required by the proposed E-APLI scheme. Nonetheless, E-APLI can still maintain a similar performance as C1D-MMSE, even without the aid of SCD. In addition, the full E-APLI has only 1dB loss in E_b/N_0 when compared with the ideal CE for a target BLER of 10^{-4}.

TABLE I

SIMULATION RESULTS OF EM-RELATED PARAMETERS.

E_b/N_0 [dB]	10	15	20	25	30	35
$\mathrm{MSE}_{\min}$ $[10^{-4}]$	9.405	3.303	1.595	1.118	0.983	0.949
$\mathrm{MSE}_{\max}$ $[10^{-4}]$	9.564	3.345	1.615	1.124	0.991	0.953
$\mathrm{MSE}_{\mathrm{std}}$ $[10^{-6}]$	2.753	0.827	0.371	0.143	0.150	0.079

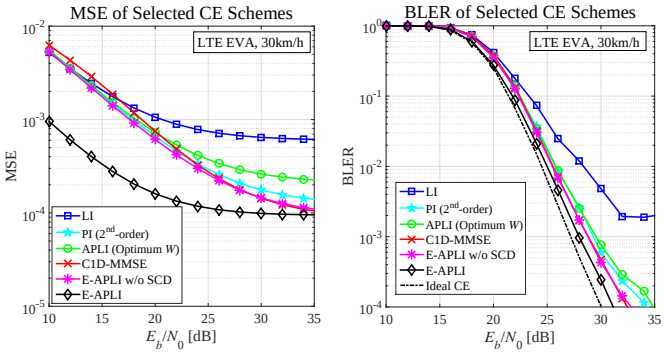

(a) MSE performance. (b) BLER performance.

Fig. 3. Performance comparison of various CE schemes.

For one OFDM symbol, the interpolation-related computational complexity of E-APLI is $\mathcal{O}(NP)$, which is the same as those of LI and APLI, where $\mathcal{O}(\cdot)$ denotes the asymptotical upper bound. The SCD module in E-APLI has a complexity of $\mathcal{O}(LNP + NP\log(NP))$, where L is the number of EM iterations which is typically less than 30 in our simulations. In contrast, C1D-MMSE yields a higher complexity of $\mathcal{O}((N_{\mathrm{MMSE}}^{\mathrm{FD}\ 3} + N_{\mathrm{MMSE}}^{\mathrm{TD}\ 3})NP)$, while providing a performance similar to [2] that has a complexity of $\mathcal{O}(N^3P)$.

V. CONCLUSIONS

In this letter, we propose the E-APLI-CE scheme consisting of the new EOO, AAG and SCD procedures, significantly improving the conventional APLI-CE method. EOO exploits the new ABI/PBI submodules to improve the EO's accuracy, while AAG better fits the channel estimates to the FD-CTF contour. In addition, SCD utilizes channel characteristics for performance enhancement. Simulation results prove the superiority of E-APLI-CE over a range of existing schemes.

REFERENCES

[1] M. Jiang, J. Akhtman and L. Hanzo, "Iterative joint channel estimation and multi-user detection for multiple-antenna aided OFDM systems," *IEEE Transactions on Wireless Communications*, vol. 6, no. 8, pp. 2904–2914, Aug. 2007.

[2] G. Liu, L. Zeng, H. Li, L. Xu, and Z. Wang, "Adaptive interpolation for pilot-aided channel estimator in OFDM system," *IEEE Transactions on Broadcasting*, vol. 60, no. 3, pp. 486–498, Sept. 2014.

[3] L. Hanzo, M. Münster, and B. J. Choi, *OFDM and MC-CDMA for broadband multi-user communications, WLANs and broadcasting*. Reading, Massachusetts: Wiley, 2004.

[4] W. Hou and M. Jiang, "Channel estimation for AF-type cooperative OFDM systems with low pilot overhead," *IEEE Signal Processing Letters*, vol. 19, no. 10, pp. 651–654, Oct. 2012.

[5] M. Jiang, S. Huang, and W. Wen, "Adaptive polar-linear interpolation aided channel estimation for wireless communication systems," *IEEE Transactions on Wireless Communications*, vol. 11, no. 3, pp. 920–926, Mar. 2012.

[6] X. Chen and M. Jiang, "Adaptive statistical Bayesian MMSE channel estimation for visible light communication," *IEEE Transactions on Signal Processing*, vol. 65, no. 5, pp. 1287–1299, Mar. 2017.

[7] S. Park, J. W. Choi, J. Y. Seol, and B. Shim, "Expectation-maximization-based channel estimation for multiuser MIMO systems," *IEEE Transactions on Communications*, vol. 65, no. 6, pp. 2397–2410, June 2017.

[8] 3GPP, "3rd generation partnership project; technical specification group radio access network; spatial channel model for multiple input multiple output (MIMO) simulations (release 15)," TR 25.996 V15.0.0, June 2018.

[9] ——, "3rd generation partnership project; technical specification group radio access network; evolved universal terrestrial radio access (E-UTRA); physical channels and modulation (release 15)," TS 36.211 V15.2.0, July 2018.